Supramolecular Assembly of H-Bonded Side-Chain Polymers Containing Conjugated Pyridyl H-Acceptor Pendants and Various Low-Band-Gap H-Donor Dyes Bearing Cyanoacrylic Acid Groups for Organic Solar Cell Applications

TZUNG-CHI LIANG,[1] I-HUNG CHIANG,[1] PO-JEN YANG,[1] DHANANJAY KEKUDA,[2] CHIH-WEI CHU,[2,3] HONG-CHEU LIN[1]

[1]Department of Materials Science and Engineering, National Chiao Tung University, Hsinchu, Taiwan, Republic of China

[2]Research Center for Applied Sciences, Academia Sinica, Taipei, Taiwan, Republic of China

[3]Department of Photonics, National Chiao Tung University, Hsinchu, Taiwan, Republic of China

Received 8 June 2009; accepted 14 July 2009
DOI: 10.1002/pola.23643
Published online in Wiley InterScience (www.interscience.wiley.com).

ABSTRACT: Novel supramolecular side-chain polymers were constructed by complexation of proton acceptor (H-acceptor) polymers, i.e., side-chain conjugated polymers **P1–P2** containing pyridyl pendants, with low-band-gap proton donor (H-donor) dyes **S1–S4** (bearing terminal cyanoacrylic acids) in a proper molar ratio. Besides unique mesomorphic properties confirmed by DSC and XRD results, the H-bonds of supramolecular side-chain structures formed by pyridyl H-acceptors and cyanoacrylic acid H-donors were also confirmed by FTIR measurements. H-donor dyes **S1–S4** in solid films exhibited broad absorption peaks located in the range of 471–490 nm with optical band-gaps of 1.99–2.14 eV. Furthermore, H-bonded polymer complexes **P1/S1–P1/S4** and **P2/S1–P2/S4** exhibited broad absorption peaks in the range of 440–462 nm with optical band-gaps of 2.11–2.25 eV. Under 100 mW/cm^2 of AM 1.5 white-light illumination, the bulk heterojunction polymer solar cell (PSC) devices containing an active layer of H-bonded polymer complexes **P1/S1–P1/S4** and **P2/S1–P2/S4** (as electron donors) mixed with [6,6]-phenyl C_{61} butyric acid methyl ester (i.e., PCBM, as an electron acceptor) in the weight ratio of 1:1 were investigated. The PSC device containing H-bonded polymer complex **P1/S3** mixed with PCBM (1:1 w/w) gave the best preliminary result with an overall power conversion efficiency (PCE) of 0.50%, a short-circuit current of 3.17 mA/cm^2, an open-circuit voltage of 0.47 V, and a fill factor of 34%. © 2009 Wiley Periodicals, Inc. J Polym Sci Part A: Polym Chem 47: 5998–6013, 2009
Keywords: dyes/pigments; H-bonded polymer complex; liquid-crystalline polymers (LCP); low-band-gap dye; polymer solar cell; supramolecular polymer; supramolecular structures

INTRODUCTION

Self-assembled phenomena through molecular recognition between complementary constituents have been explored in various areas, such as the

Additional Supporting Information may be found in the online version of this article.

Correspondence to: H.-C. Lin (E-mail: linhc@cc.nctu.edu.tw)

Journal of Polymer Science: Part A: Polymer Chemistry, Vol. 47, 5998–6013 (2009)
© 2009 Wiley Periodicals, Inc.

applications of biomaterials, liquid crystalline (LC) materials, and electro-optical materials.[1–8] Not only innovative LC properties of novel supramolecules consisting of two counterparts can be generated through intermolecular hetero-hydrogen-bonding interactions, but also particular self-assembly of nanoscaled building blocks using noncovalent interactions (e.g., hydrogen bonding, acid/base proton transfer, and electrostatic forces) may be amplified into macroscopically observable phenomena.[9] More recently, direct energy harvesting from sunlight by using photovoltaic cells (PVCs) has increasingly attracted intensified attention to utilize renewable energy of the nature, especially for the development of organic solar cells.[10–12] Compared with inorganics (such as Si), organic materials (especially polymers) have the benefits to be easily made into devices with light weight, large area, and flexible panels, so different concepts of solar cell architectures have been developed by organics, including blends of polymers[13–20] and block copolymers[21] with [6,6]-phenyl C_{61} butyric acid methyl ester (i.e., PCBM, as an electron acceptor). Among the organic solar cell materials investigated so far, semiconducting conjugated polymers with electron donor–acceptor architectures are one of the most effective ways to build intramolecular charge transfer (ICT) interaction between the electron donor (D) and electron acceptor (A) segments.[22–30] Conjugated D-A copolymers with strong ICT effects are promising materials for the development of high performance polymer-based PVCs due to the merits of narrow band-gaps,[25–27] broad absorption bands extending into the near-infrared spectral range, efficient photoinduced charge transfer and separation, pronounced charge photogeneration and collection, and high mobility of ambipolar charge transport.[28–30] Furthermore, different concepts of solar cell architectures, including the dye blends containing inorganics (PCBM, TiO_2, and ZnO as electron acceptors)[31] and/or polymers,[32–34] have been successfully progressed the efficiencies of the bulk heterojunction polymer solar cell (PSC) devices. However, due to the aggregations of the dyes originated from their strong π–π interactions, the power conversion efficiency (PCE) values of PSC devices are limited by the dye contents in the polymer blends. Therefore, the H-bonded interactions of supramolecular polymers in this work can be introduced to reduce the aggregations of the low-band-gap organic dyes (as H-donors), and thus, to improve the PCE values for the organic solar cell applications.

It is noticeable that the well-known electron-withdrawing unit would be an aryl-substituted cyano or nitro group, which has been widely utilized in organic solar cell materials, including metal-free dye sensitized solar cell (DSSC) materials.[35] On account of the electron-rich sulfur and nitrogen atoms, especially in heterocyclic structures, polymers, and organic molecules[36,37] containing carbazole, triphenylamine, and thiophene units as the electron-donating moieties have lately attracted considerable interests in the applications of light-emitting diodes,[38,39] photovoltaic devices,[40,41] and organic field effect transistors (OFETs).[42] In the past years, various attempts have been made to increase the delocalization of π-electrons by constructing more coplanar conjugated systems to generate low-band-gap dyes. Another approach is to incorporate electron-accepting (A) units (e.g., cyano or nitro groups) with electron-donating (D) units (e.g., carbazole or triphenylamine groups) to produce low-band-gap dyes with resonance structures (i.e., D-A $\leftrightarrow$ D^+A^-).[43,44] Recently, Lin and coworkers have introduced some novel conjugated spacers by inserting benzothiadiazole, benzoselenadiazole, and 1*H*-phenanthro[9,10-*d*]imidazole segments into low-band-gap dyes (bearing D-A structures) for the applications of photovoltaic devices.[45,46]

To incorporate low-band-gap organic dyes (as H-donors) into supramolecular polymers for organic solar cell applications, conjugated pyridyl H-acceptors were integrated into the side-chain polymeric structures as the pendent groups rather than as small molecules (acting as luminescent chromophores) in our previous studies.[47–50] As shown in the schematic illustration of Figure 1, supramolecular side-chain polymers (i.e., H-bonded polymer complexes) were constructed by complexation of pyridyl H-acceptor polymers, i.e., side-chain polymers **P1–P2** containing conjugated pyridyl pendants, with low-band-gap H-donor dyes **S1–S4** (bearing terminal cyanoacrylic acids) in a molar ratio of 1:1 for pyridyl and acid units, which would have much more uptaken loads of photovoltaic dyes in the supramolecular polymeric structures (without phase separation) compared with the normal polymer blends. Our detailed investigations will prove that larger aggregations of the acid protected dyes occurred in the polymer blends due to the lack of supramolecular interactions, and a polymer blend of the conjugated H-acceptor polymer **P1** and the acid-protected dye **S1P** (refer Fig. S1 of the Supporting Information) illustrated an obvious reduction in the PCE value

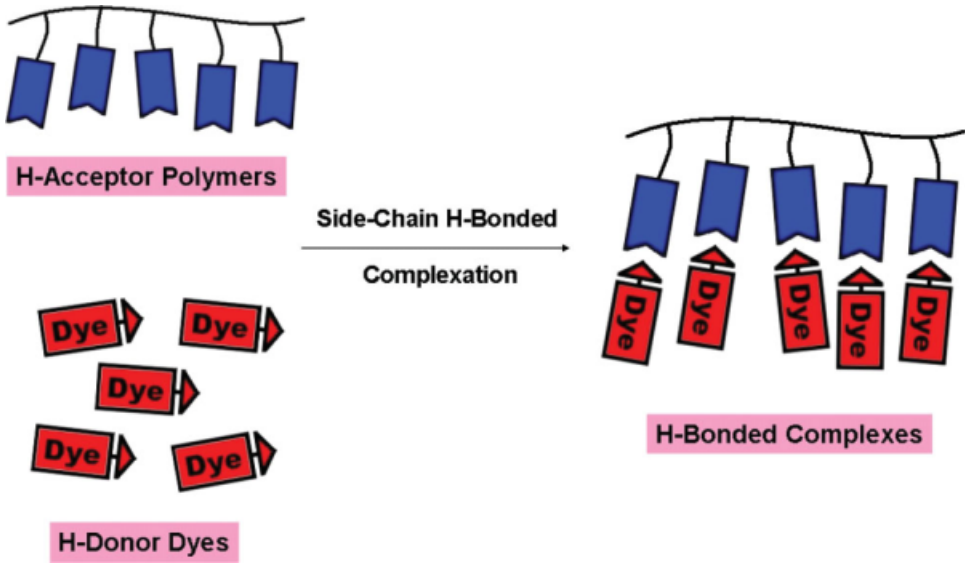

Figure 1. Schematic illustration of complexation processes for H-bonded side-chain polymers. [Color figure can be viewed in the online issue, which is available at www.interscience.wiley.com.]

in contrast to the supramolecular analogue **P1/S1**. Different molar ratios of conjugated H-acceptor monomer **PBB** (containing a pyridyl terminus) and hole-transporting monomer **CAZ** (bearing a carbazole unit) were copolymerized through free radical polymerization to obtain H-acceptor polymers (**P1** and **P2**). Both terminal carbazole or triphenylamine groups as electron-donating (D) units were in conjunction with cyanoacrylic acid groups as electron-accepting (A) units to yield low-band-gap H-donor dyes **S1–S4**, which were bridged through various numbers of fluorene, bithiazole, and thiophene units (refer Fig. 2). By incorporating side-chain conjugated H-acceptor polymers with low-band-gap H-donor dyes, the LC and PVC properties of the supramolecular polymer complexes can be easily adjusted. The present investigation is mainly to explore the supramolecular structures of H-bonded side-chain polymers containing low-band-gap H-donor dyes for the PSC applications. Therefore, the bulk heterojunction PSC devices containing an active layer of H-bonded polymer complexes **P1/S1–P1/S4** and **P2/S1–P2/S4** (as electron donors) mixed with PCBM (as an electron acceptor) were evaluated.

EXPERIMENTAL

Materials

Chemicals and solvents were reagent grades and purchased from Aldrich, ACROS, TCI, and Lancaster Chemical. Dichloromathane and THF were distilled to keep anhydrous before use. The other chemicals were used without further purification. The synthetic routes of side-chain conjugated H-acceptor polymers **P1** and **P2** (as shown in Fig. 2) were reported in our previous publication.[51] Synthesis and characterization of H-donor dyes **S1–S4** and their intermediates (refer Fig. 2) are described in the Supporting Information. The chemical structures for all products were confirmed by ^{1}H NMR spectroscopy and elemental analyses.

Preparation of Supramolecular Polymer Complexes

In all cases, all H-donor dyes and H-acceptor polymers (as shown in Fig. 2) were dissolved in THF to make a clear solution. After then, most of the solvents were evaporated under ambient conditions, which were followed by drying in a vacuum oven at 60 °C for several hours. The complexation of H-donor acids and H-acceptor polymers through hydrogen bonding was proceeded during the solvent evaporation. The H-bonded side-chain polymers of all H-acceptor polymers complexed with H-donor dyes **S1–S4** had the equal molar amount of pyridyl H-acceptor and carboxylic acid H-donor groups (in 1:1 M ratio) to form supramolecular polymer complexes (i.e., H-bonded side-chain polymers).

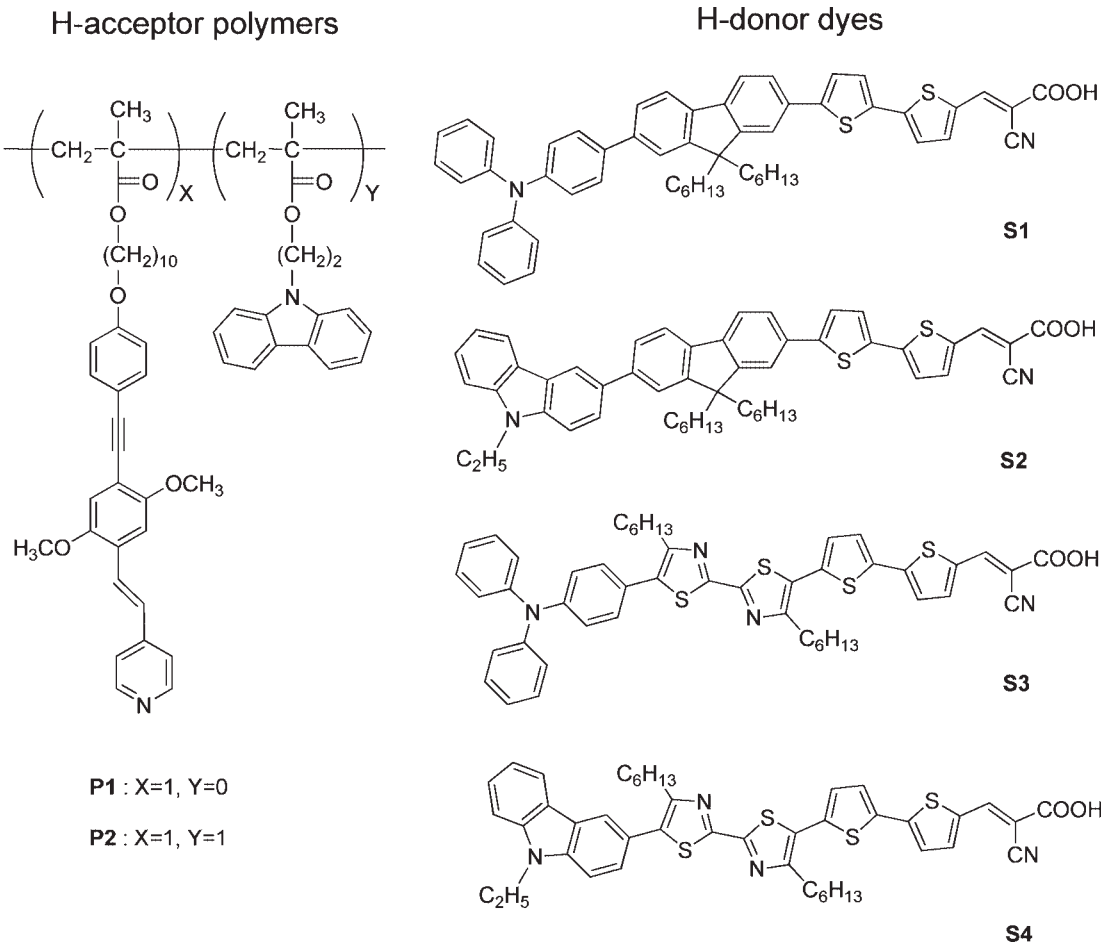

Figure 2. H-acceptor polymers (**P1** and **P2**) and H-donor dyes (**S1**–**S4**) used in the H-bonded polymer complexes (**P1/S1**–**P1/S4** and **P2/S1**–**P2/S4**).

Measurements and Characterization

^{1}H NMR spectra were recorded on a Varian unity 300 MHz spectrometer using *d*-DMSO as solvents. Elemental analyses were proceeded on a HERAEUS CHN-OS RAPID elemental analyzer. Fourier transform infrared (FT-IR) spectra were performed on a Nicolet 360 FT-IR spectrometer. The textures of mesophases were characterized by a polarizing optical microscope (POM, model: Leica DMLP) equipped with a hot stage. Temperatures and enthalpies of phase transitions were determined by differential scanning calorimetry (DSC, model: Perkin–Elmer Pyris 7) at a heating and cooling rate of 10 °C/min under nitrogen. Thermogravimetric analyses (TGA) were conducted on a Du Pont Thermal Analyst 2100 system with a TGA 2950 thermogravimetric analyzer at a heating rate of 20 °C/min under nitrogen. Gel permeation chromatography (GPC) analyses were executed with a Water 1515 separations module using polystyrene as a standard and THF as an eluant. UV-visible absorption spectra were recorded in dilute THF solutions (10^{-6} M) on a HP G1103A spectrophotometer, and photoluminescence (PL) spectra were obtained on a Hitachi F-4500 spectrophotometer. Thin films of UV-vis and PL measurements were spin-coated on quartz substrates from THF solutions with a concentration of 1 wt %. Cyclic voltammetry (CV) measurements were carried out using a BAS 100 electrochemical analyzer with a standard three-electrode electrochemical cell in a 0.1 M tetrabutylammonium hexafluorophosphate [(TBA)PF_6] solution (in acetonitrile) at room temperature with a scanning rate of 50 mV/s. During the CV measurements, the solutions were purged with nitrogen for 30 s. In each case, a carbon working electrode coated with a thin layer of copolymers, a platinum wire as the counter electrode, and a silver wire as the quasi-reference electrode were used, and Ag/AgCl (3 M KCl) electrode was served as a

reference electrode for all potentials quoted herein. The redox couple of ferrocene/ferrocenium ion (Fc/Fc^+) was used as an external standard. The corresponding highest occupied molecular orbital (HOMO) and lowest unoccupied molecular orbital (LUMO) levels were calculated using E_{ox}/onset and E_{red}/onset for experiments in solid films of H-acceptor polymers (**P1** and **P2**), H-donor dyes (**S1–S4**), and H-bonded polymer complexes (**P1/S1–P1/S4** and **P2/S1–P2/S4**), which were performed by drop-casting films with a similar thickness from THF solutions (~5 mg/mL). The LUMO level of PCBM used was in accordance with the literature datum.[52] The onset potentials were determined from the intersections of two tangents drawn at the rising currents and background currents of the cyclic voltammetry (CV) measurements. Synchrotron powder X-ray diffraction (XRD) measurements were performed at beamline BL17A of the National Synchrotron Radiation Research Center (NSRRC) in Taiwan, where the X-ray wavelength used was 1.33,366 Å. XRD data were collected using imaging plates (IP, of an area = 20×40 cm^2 and a pixel resolution of 100) curved with a radius equivalent to the sample-to-image plate distance of 280 mm, and the diffraction signals were accumulated for 3 min. The powder samples were packed into a capillary tube and heated by a heat gun, where the temperature controller was programmable by a PC with a PID feed back system. The scattering angle theta values were calibrated by a mixture of silver behenate and silicon.

Device Fabrication and Characterization of PSCs

The PSC devices in this study were composed of an active layer of blended H-bonded side-chain polymers (**P1/S1–P1/S4** and **P2/S1–P2/S4**) mixed with [6,6]-phenyl C_{61} butyric acid methyl ester (i.e., PCBM) in solid films, which was sandwiched between a transparent indium tin oxide (ITO) anode and a metal cathode. Before device fabrication, ITO-coated glass substrates (1.5×1.5 cm^2) were ultrasonically cleaned in detergent, deionized water, acetone, and isopropyl alcohol. Afterward, the substrates were treated with UV ozone for 15 min, and a layer of poly(ethylene dioxythiophene): polystyrenesulfonate (PEDOT:PSS, ~30 nm) was subsequently spin-coated onto the substrates. After baking at 130 °C for 1 h, the substrates were transferred to a nitrogen-filled glovebox. The PSC devices were fabricated by spin-coating solutions of blended H-bonded polymer complexes:PCBM (with various weight ratios) onto the PEDOT:PSS modified substrates at 600 rpm for 60 s (~200 nm), and placed in a covered glass Petri dish. Initially, the blended solutions were prepared by dissolving both H-bonded polymer complexes (**P1/S1–P1/S4** and **P2/S1–P2/S4**) and PCBM (with a 1:1 weight ratio initially and then with various weight ratios for the optimum H-bonded polymer complex) in chlorobenzene (20 mg/1 mL), followed by continuous stirring for 12 h at 50 °C. In the slow-growth approach, blended H-bonded polymer complexes in solid films were kept in the liquid phase after spin-coating by using the solvent (chlorobenzene) with a high boiling point. Finally, a calcium layer (30 nm) and a subsequent aluminum layer (100 nm) were thermally evaporated through a shadow mask at a pressure below 6×10^{-6} Torr, and the active area of the device was 0.12 cm^2. All PSC devices were prepared and measured under ambient conditions.

RESULTS AND DISCUSSION

FT-IR Spectroscopy of H-Bonded Polymer Complexes

All H-bonded side-chain polymers consisting of the appropriate molar ratio (fully H-bonded complexes in a molar ratio of 1:1 for pyridyl and acid units) of H-acceptor polymers (**P1** and **P2**) and H-donor dyes (**S1–S4**) were prepared by slow evaporation of THF solutions and followed by drying *in vacuo*. The formation of hydrogen bonding in supramolecular side-chain polymers containing H-donor dyes (**S1–S4**) was confirmed by FT-IR spectroscopy. As shown in Figure 3, IR spectra of H-acceptor polymer **P2**, H-donor dye **S1**, and H-bonded complex **P2/S1** are compared to analyze the hydrogen bonds in the supramolecular structure of H-bonded polymer complex **P2/S1**. In contrast to the O—H band of pure **S1** at 2640 and 2510 cm^{-1}, the weaker O—H band observed at 2497 and 1902 cm^{-1} in H-bonded polymer complex **P2/S1** is indicative of stronger hydrogen bonding between the pyridyl group of **P2** and the carboxylic acid of **S1** in the H-bonded complex. On the other hand, a C=O stretching vibration appeared at 1722 cm^{-1} in H-bonded polymer complex **P2/S1**, which shows that the carbonyl group was in a less associated state than that in pure **S1** with a weaker C=O stretching vibration appeared at 1690 cm^{-1}. Both results suggest that hydrogen bonds were formed between H-acceptor

polymer **P2** and H-donor dye **S1** in the solid state of H-bonded polymer complex **P2/S1**. The other H-bonded polymer complexes also have the similar consequences of H-bonding formation as the H-bonded complex demonstrated here.[53] However, in comparison with H-bonded polymer complex **P1/S1**, physical blend **P1/S1P** (without H-bonds) in Figure S2 (refer the Supporting Information) shows a weaker C=O stretching vibration appeared at 1706 cm^{-1} for lack of H-bonding interactions.

Phase Behavior

The phase transition temperatures of H-acceptor polymers (**P1** and **P2**), H-donor dyes (**S1–S4**), and H-bonded side-chain polymers (i.e., H-bonded polymer complexes **P1/S1–P1/S4** and **P2/S1–P2/S4**) are summarized in Table 1, which were determined by DSC (under nitrogen) and POM. The weight-average molecular weights (M_w) of H-acceptor polymers **P1** and **P2** (determined by GPC) are 14,400 g/mol (PDI = 1.72) and 38,100 g/mol (PDI = 3.24), respectively. The glass transition temperatures (T_g) of H-acceptor polymers **P1** and **P2** are 63 and 88 °C, respectively.[51] To elucidate the H-bonding effect of H-bonded pendants on the thermal properties of supramolecular side-chain polymers, H-donor dyes **S1–S4** were introduced to be incorporated with H-acceptor side-chain polymers **P1** and **P2**. As shown in Table 1, both series of H-bonded complexes containing H-acceptor polymers **P1** and **P2** showed only a single glass transition, which suggests good miscibilities between H-donor dyes (i.e., **S1–S4**) and H-acceptor polymers (i.e., **P1** and **P2**).

Since no melting and crystallization transitions were observed in the DSC measurements, it suggests that these H-bonded complexes possess amorphous characteristics. However, the T_g values of the H-bonded complexes are notably higher than those of their corresponding H-acceptor polymers **P1** and **P2**. The increases of T_g values in H-bonded complexes are probably due to the larger π–π interactions originated from the increased rigid-rod lengths of the integrated H-bonded pendants (containing both pyridyl H-acceptor units and H-donor dyes). In contrast to H-acceptor homopolymer **P1** and its H-bonded complexes, H-acceptor copolymer **P2** and its H-bonded complexes possessed higher T_g values due to the integration of more bulky and rigid **CAZ** components in copolymer **P2**. Comparing the H-bonded complexes containing fluorene-linked dyes (**S1** and **S2**) and bithiazole-linked dyes (**S3** and **S4**), owing to the higher rigidity of bithiazole units in H-donor dyes **S3** and **S4**, the latter H-bonded complexes (**P1–P2/S3** and **P1–P2/S4**) have higher T_g values than the former H-bonded complexes (**P1–P2/S1** and **P1–P2/S2**), respectively. This obviously indicates that the rigid bithiazole linkers will enhance the aggregation of the pendants in the H-bonded complexes effectively. In contrast to the H-bonded complexes (**P1–P2/S1** and **P1–P2/S3**) containing end-capping triphenylamine dyes (**S1** and **S3**), owing to the higher rigidity and coplanarity of end-capping cabazole units in H-donor dyes (**S2** and **S4**), the analogous H-bonded complexes (**P1–P2/S2** and **P1–P2/S4**) containing end-capping cabazole dyes (**S2** and **S4**) have higher T_g values.

The isotropization temperatures (T_i) have the similar trends as the glass transition temperatures (T_g) in H-bonded polymer complexes (**P1/S1–P1/S4** and **P2/S1–P2/S4**). Moreover, comparing analogous H-bonded complexes consisting of the same H-donor dyes, H-bonded complexes containing H-acceptor homopolymer **P1** possess the higher isotropization temperatures (T_i) and the broader mesophasic ranges than those containing H-acceptor copolymer **P2**. In addition, compared with H-bonded polymer complexes **P1/S1** and **P1/S2** bearing fluorene-linked dyes (**S1** and **S2**), H-bonded polymer complexes **P1/S3** and **P1/S4** bearing bithiazole-linked dyes (**S3** and **S4**) have higher T_i values and broader mesophasic ranges. In general, the isotropization temperatures (T_i) and mesophasic ranges of H-bonded side-chain polymers would be enhanced while the H-bonded central cores are longer and more rigid.

As shown in Figure 4(a), the mesomorphic behavior of H-bonded polymer complex **P2/S4** (cooling at 130 °C) was confirmed as the nematic phase by the schlieren texture of POM, which was further elucidated by X-ray diffraction (XRD) measurements in Figure 4(b) that no sharp d-spacing values, i.e., no layered structures of the smectic phase, were observed in the XRD intensity against angle profiles of H-bonded polymer complexes **P1/S1** and **P2/S4** at 130 °C (in the mesophasic range). According to the POM and XRD measurements, H-acceptor homopolymer **P1** and all H-bonded polymer complexes (**P1/S1–P1/S4** and **P2/S1–P2/S4**) in Table 1 were verified to possess the nematic phase, but H-acceptor copolymer **P2** bearing 50% molar ratio of **CAZ** units did not possess any mesophase. Hence, the integration of **CAZ** units in copolymer **P2** is detrimental

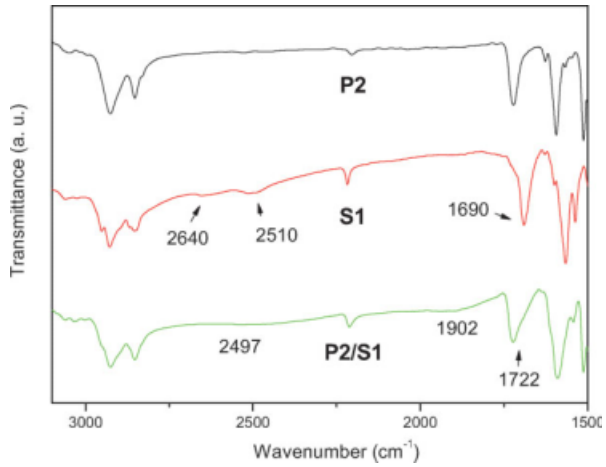

Figure 3. FTIR spectra of H-acceptor polymer **P2**, H-donor dye **S1**, and H-bonded polymer complex **P2/S1**.

to the formation of the mesophase, which can be explained by that the **CAZ** units with nonmesomorphic property may dilute and hinder the molecular packing of the LC arrangements in copolymer **P2**. However, the nematic phase was introduced to the corresponding H-bonded polymer complexes (**P2/S1–P2/S4**) of copolymer **P2** due to the extended H-bonded mesogens by combination of H-acceptor pedants with H-donor dyes. Moreover, the mesophasic ranges and T_i values of the H-bonded polymer complexes (**P2/S1–P2/S4**) containing copolymer **P2** were apparently reduced by the **CAZ** units of H-acceptor copolymer **P2**, which diluted and interfered the LC arrangements of the H-bonded mesogens in their subsequent H-bonded polymer complexes. However, acid-protected dye **S1P** and physical blend **P1/S1P** (without H-bonds) have lower phase transition temperatures (including the isotropization temperature T_i) than H-bonded polymer complex **P1/S1** due to the dilution effect of the acid-protected dye **S1P** moieties in the physical blend **P1/S1P** (refer Table S1 of the Supporting Information).

Table 1. Thermal Properties of H-Acceptor Polymers **(P1–P2)**, H-Donor Dyes **(S1–S4)**, and H-Bonded Polymer Complexes **(P1/S1–P1/S4** and **P2/S1–P2/S4)**

Compound	Phase Transitions (°C)[a,b]
P1	G 63 N 125[c] I
P2	G 88 K 110[c] I
S1	K 156 (10.8) I
S2	K 163 (13.4) I
S3	K 173 (25.9) I
S4	K 180 (26.3) I
P1/S1	G 87 N 151[c] I
P1/S2	G 89 N 155[c] I
P1/S3	G 96 N 167[c] I
P1/S4	G 99 N 172[c] I
P2/S1	G 96 N 141[c] I
P2/S2	G 98 N 147[c] I
P2/S3	G 104 N 156[c] I
P2/S4	G 105 N 162[c] I

[a] Phase transition temperatures (°C) and enthalpies (in parentheses, kJ/mol) were determined by DSC at a heating rate of 10 °C/min.
[b] G, glassy state; K, crystalline; N, nematic; I, isotropic.
[c] Phase transition temperatures were obtained by POM and confirmed by XRD.

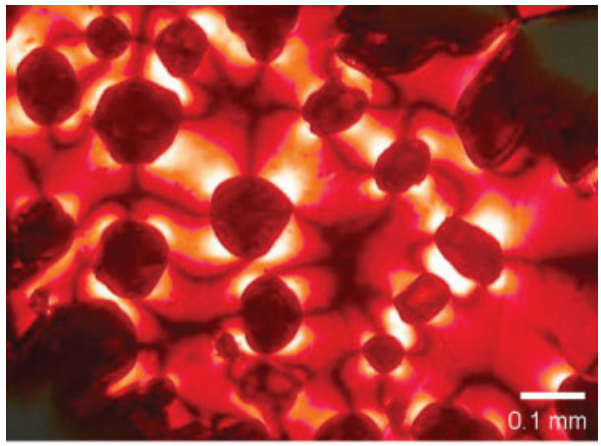

(a)

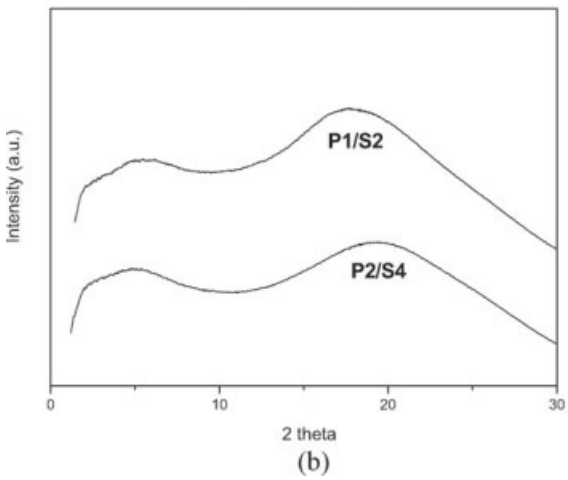

(b)

Figure 4. (a) Optical texture of the nematic phase in H-bonded polymer complex **P2/S4** observed by POM at 130 °C (cooling) and (b) XRD intensity against angle profiles obtained from H-bonded polymer complexes **P1/S1** and **P2/S4** at 130 °C (in the nematic phase).

Table 2. Absorption and Photoluminescence Spectral Data of H-Acceptor Polymers **(P1–P2)**, H-Donor Dyes **(S1–S4)**, and H-Bonded Polymer Complexes **(P1/S1–P1/S4** and **P2/S1–P2/S4)**

Compound	$\lambda_{abs,sol}$[a] (nm)	$\lambda_{abs,film}$[a] (nm)	$\lambda_{PL,film}$ (nm)
P1	385	393	496
P2	385	393	487
S1	460	471	631
S2	462	478	638
S3	458	481	668
S4	460	490	677
P1/S1	–	440	614
P1/S2	–	445	621
P1/S3	–	462	640
P1/S4	–	451	645
P2/S1	–	440	611
P2/S2	–	448	618
P2/S3	–	457	638
P2/S4	–	452	638

[a] Absorption and PL emission spectra were recorded in dilute THF solutions.

Optical Properties

The UV-visible absorption spectra of H-acceptor polymers **P1**–**P2** and H-donor dyes **S1**–**S4** (in both THF solutions and solid films), and H-bonded polymer complexes **P1/S1–P1/S4** and **P2/S1–P2/S4** (in solid films) are displayed in Figures 5 and 6, and their photophysical properties are demonstrated in Table 2. The absorption energy band-gaps of H-bonded polymer complexes (**P1/S1–P1/S4** and **P2/S1–P2/S4**) could be easily tuned by the introduction of H-donor dyes (**S1–S4**), and their absorption spectra covered broad wavelength ranges for both solutions and solid films. As shown in Figure 5, the maximum absorption wavelength (λ_{abs}) of H-acceptor polymers **P1**–**P2** in THF solutions and solid films were 385 and 393 nm, respectively, which were mainly contributed from the **PBB** units. The maximum absorption wavelength (λ_{abs}) of H-donor dyes **S1–S4** in THF solutions were in the range of 458–462 nm (in THF solutions) and 471–490 nm (in solid films). Because of the interchain association and π–π stacking of these polymers and dyes in solids, the absorption spectra of all H-acceptor polymers and H-donor dyes in solid films were generally larger than those in dilute solutions (i.e., 8 nm red shifts in polymers and 11–30 nm red shifts in dyes). After complexation (in solid films as shown in Fig. 6), H-bonded polymer complexes **P1/S1–P1/S4** and **P2/S1–P2/S4** displayed blue-shifted absorption peaks (at 440–462 nm) in contrast to H-donor dyes **S1–S4**. The blue shifted absorption (blue shifted wavelength $\Delta\lambda_{abs}$ = 19–39 nm) was due to the dilution effect of H-acceptor polymers as solid solvents for dyes (as solutes) in solid H-bonded polymer complexes. Compared with the H-bonded complexes containing fluorene-linked dyes (**S1** and **S2**), the corresponding H-bonded complexes containing bithiazole-linked dyes (**S3** and **S4**) have longer absorption wavelengths and thus to have lower optical band-gaps, which were originated from the smaller optical band-gaps of bithiazole-linked dyes (**S3** and **S4**) in solid films. Therefore, the H-bonded complexes containing bithiazole-linked dyes (**S3** and **S4**) might have the gifts of lower optical band-gaps for further good performance in photovoltaic properties. However,

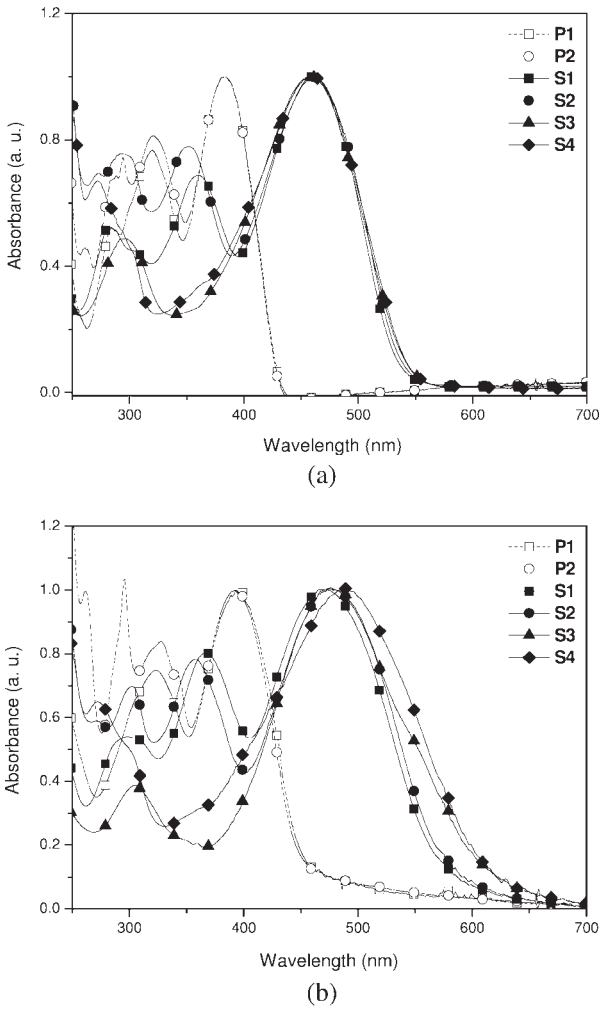

Figure 5. UV-visible absorption spectra of H-acceptor polymers **P1**–**P2** and H-donor dyes **S1–S4** (a) in THF solutions and (b) in solid films.

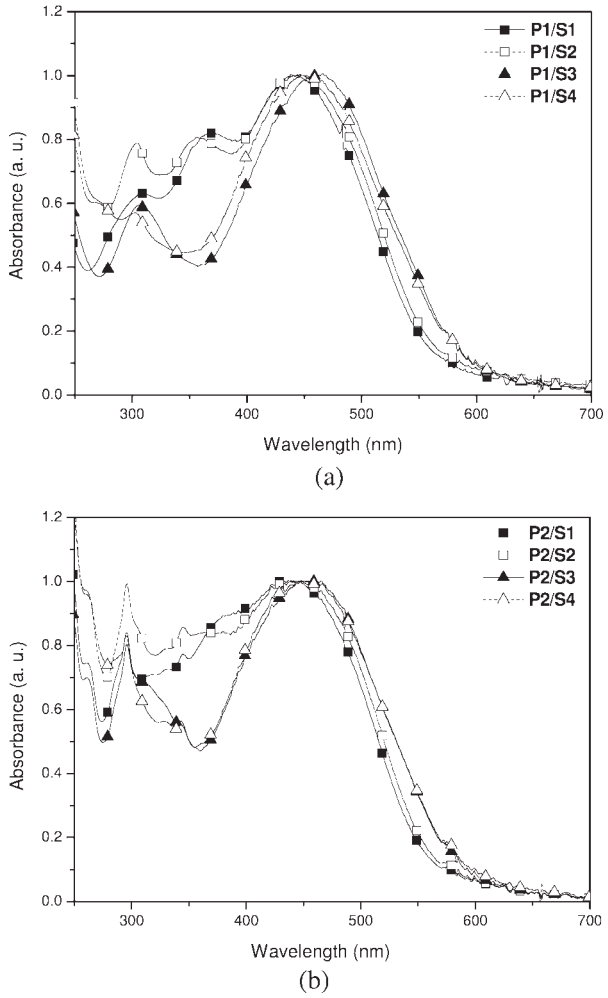

Figure 6. UV-visible absorption spectra of (a) H-bonded polymer complexes **P1/S1–P1/S4** and (b) H-bonded polymer complexes **P2/S1–P2/S4** in solid films.

due to the lack of supramolecular interactions in polymer blend **P1/S1P** and a larger aggregation of the acid-protected dye **S1P**, a red-shifted (33 nm) absorption in the solid film of polymer blend **P1/S1P** than that of H-bonded polymer complex **P1/S1** was observed (refer Fig. S3 and Table S2 of the Supporting Information).

The photoluminescence (PL) spectra of H-acceptor polymers **P1**–**P2**, H-donor dyes **S1–S4**, and H-bonded polymer complexes **P1/S1–P1/S4** and **P2/S1–P2/S4** (in solid films) are summarized in Table 1. Similar to the UV-visible absorption spectra, the PL emission wavelengths of H-bonded polymer complexes **P1/S1–P1/S4** and **P2/S1–P2/S4** (at 611–645 nm) were all blue-shifted in contrast to those of H-donor dyes **S1–S4** (at 631–677 nm). The PL emission spectra (in solid films) of the H-acceptor polymers **P1** and **P2** were dramatically quenched by adding H-donor dyes **S1–S4** in the H-bonded polymer complexes **P1/S1–P1/S4** and **P2/S1–P2/S4**. The corresponding optical quenching properties of these H-bonded complexes in solid films, including the broad optical absorptions and low optical band-gaps, proposed the potential applications in photovoltaic cells.

Electrochemical Properties

Narrow-band-gap H-bonded side-chain polymers were designed as donor–acceptor type materials by using H-donor dyes containing electron-donating carbazole and triphenylamine moieties and electron-withdrawing cyano moieties. To understand the energy band structures of these new narrow-band-gap H-bonded polymer complexes for the PSC device application, the electronic states, i.e., highest occupied molecular orbital (HOMO) and lowest unoccupied molecular orbital (LUMO) levels, of the H-bonded side-chain polymers were investigated by the cyclic voltammetry (CV) measurements. The oxidation and reduction cyclic voltammograms of H-bonded polymer complexes **P1/S1–P1/S4** and **P2/S1–P2/S4** in solid films are displayed in Figure 7. H-bonded polymer complexes **P1/S1–P1/S4** and **P2/S1–P2/S4** exhibited quasi-reversible (or reversible) oxidation and reduction peaks as evident from the areas and close proximity of the anodic and cathodic scans. The onset oxidation and reduction potentials (in solid films) of H-acceptor polymers **P1**–**P2**, H-donor dyes **S1–S4**, and H-bonded polymer complexes **P1/S1–P1/S4** and **P2/S1–P2/S4** are demonstrated Table 3. Ag/AgCl was served as a reference electrode, and it was calibrated by ferrocene ($E^{1/2}_{\text{ferrocene}} = 0.45$ mV vs. Ag/AgCl). The HOMO and LUMO energy levels were estimated by the oxidation and reduction potentials from the reference energy level of ferrocene (4.8 eV below the vacuum level) according to the following equation: $E_{\text{HOMO/LUMO}} = [-(E_{\text{onset}} - 0.45) - 4.8]$ eV. According to the previous estimation, the HOMO and LUMO energy levels as well as the band-gap values directly measured from CV ($E_{\text{g,cv}}$) of all compounds are also summarized in Table 3.

As can be seen, all band-gap values of $E_{\text{g,cv}}$ had the analogous sequences as confirmed by the optical band-gap values observed from UV-vis spectra ($E_{\text{g,opt}}$). By using the H-donor dyes with electron donor-acceptor effects, H-bonded polymer complexes **P1/S1–P1/S4** and **P2/S1–P2/S4** displayed narrower band-gaps (0.68 eV smaller in $E_{\text{g,opt}}$ and

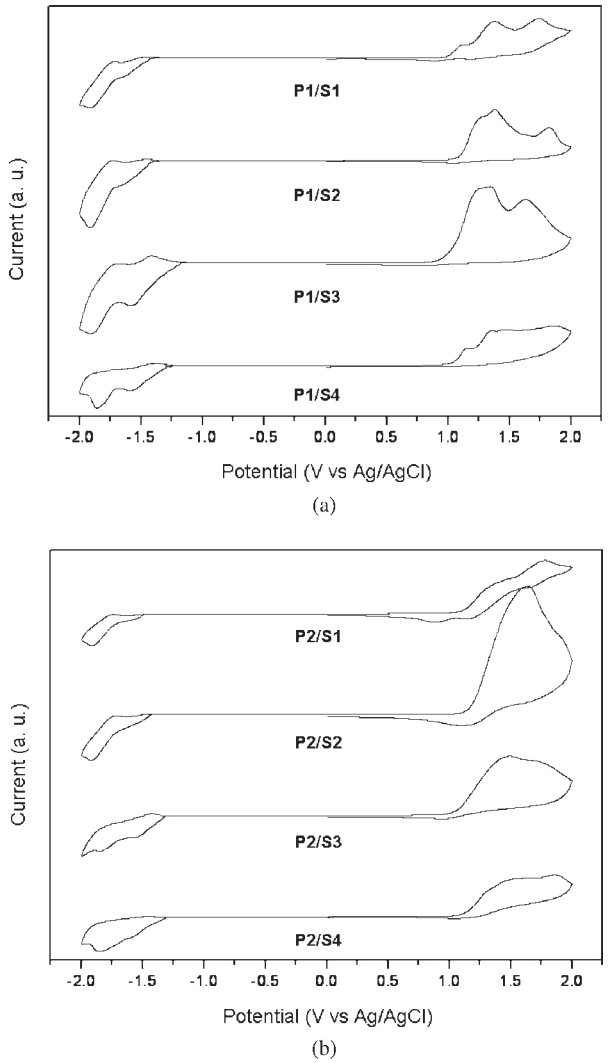

Figure 7. Cyclic voltammograms of H-bonded polymer complexes (a) **P1/S1–P1/S4** and (b) **P2/S1–P2/S4**.

0.51 eV smaller in $E_{g,cv}$) compared to H-acceptor polymers **P1–P2** (refer Table 3). However, due to the dilution results of H-acceptor polymers **P1–P2**, H-bonded polymer complexes **P1/S1–P1/S4** and **P2/S1–P2/S4** presented wider band-gaps in contrast to H-donor dyes **S1–S4**. It is worthwhile to note that the H-bonded complexes containing bithiazole-linked dyes (**S3** and **S4**) have lower optical band-gaps ($E_{g,cv}$ and $E_{g,opt}$) than the corresponding H-bonded complexes containing fluorene-linked dyes (**S1** and **S2**), which was originated from the smaller optical band-gaps of bithiazole-linked dyes (**S3** and **S4**) in solid films. Compared with H-acceptor polymers **P1–P2** and H-donor dyes **S1–S4**, the medium HOMO and LUMO energy levels of H-bonded polymer complexes (**P1/S1–P1/S4** and **P2/S1–P2/S4**) could be adjusted. Therefore, the electrochemical reductions of H-bonded complexes showed similar LUMO energy levels at about (−2.92)–(−3.04) eV, which represented to possess high electron affinities and also make these H-bonded complexes suitable donors for electron injection and transporting to PCBM acceptors (with 0.71–0.83 eV offsets in LUMO levels regarding PCBM with a LUMO level of −3.75 eV as shown in Fig. 8)[23(b)] for the polymeric bulk heterojunction solar cell devices. On the basis of the oxidation potential data, the introduction of electron-withdrawing cyano groups in H-donor dyes to the H-bonded complexes can induce the decreases of HOMO energy levels at about (−5.36)–(−5.52) eV, which represented to possess high hole transporting properties and also make these H-bonded complexes suitable donors for hole injection and transporting to PEDOT:PSS layer and then to ITO electrode (with 0.06–0.22 eV offsets in HOMO levels regarding PEDOT:PSS layer with a HOMO level of −5.3 eV as illustrated in Fig. 8)[23(b)] for the polymeric bulk heterojunction solar cell devices.[54] Thus, the electrochemical properties of H-bonded complexes could be adjusted by introducing electron-withdrawing cyano groups and electron-donating amine groups of H-donor dyes to the H-bonded complexes, which can reduce the HOMO energy levels and increase the LUMO energy levels of the H-bonded side-chain polymers, and thus, to have narrower band-gaps.

Photovoltaic Cell Properties

The design and syntheses of the H-bonded side-chain polymers **P1/S1–P1/S4** and **P2/S1–P2/S4** is to utilize new narrow band-gap H-donor dyes self-assembled with side-chain conjugated H-acceptor polymers into supramolecular polymeric structures for the PSC applications. To investigate the potential use of H-bonded complexes in PSCs, bulk heterojunction PSC devices with a configuration of ITO/PEDOT:PSS/H-bonded polymer complexes:PCBM (1:1 w/w)/Ca/Al were fabricated from an active layer where H-bonded complexes were blended with a complementary fullerene-based electron acceptor PCBM in a weight ratio of 1:1 (w/w) initially (and later followed with various weight ratios for the optimum H-bonded polymer complex). The PSC devices were measured under AM 1.5 illumination for a calibrated solar simulator with an intensity of 100 mW/cm^2. The preliminarily photovoltaic properties are summarized in Table 4, and the typical *I–V* characteristics of all

Table 3. Electrochemical Potentials and Energy Levels of H-Acceptor Polymers (**P1–P2**), H-Donor Dyes **(S1–S4)**, and H-Bonded Polymer Complexes **(P1/S1–P1/S4** and **P2/S1–P2/S4)**

Compound	$\lambda_{onset,abs}$ (nm)[a]	$E_{g,opt}$ (eV)[a]	E_{ox} (eV)[b]	HOMO (eV)[c]	E_{re} (eV)[b]	LUMO (eV)[c]	$E_{g,cv}$ (eV)
P1	445	2.79	1.18	−5.53	−1.67	−2.68	2.85
P2	445	2.79	1.17	−5.52	−1.65	−2.70	2.82
S1	580	2.14	0.96	−5.31	−1.47	−2.88	2.43
S2	587	2.11	1.04	−5.39	−1.40	−2.95	2.44
S3	622	1.99	1.00	−5.35	−1.33	−3.02	2.33
S4	620	2.00	1.03	−5.38	−1.30	−3.05	2.33
P1/S1	552	2.25	1.01	−5.36	−1.43	−2.92	2.44
P1/S2	558	2.22	1.09	−5.44	−1.40	−2.95	2.49
P1/S3	584	2.12	1.01	−5.36	−1.33	−3.02	2.34
P1/S4	586	2.11	1.04	−5.39	−1.32	−3.03	2.36
P2/S1	554	2.24	1.09	−5.44	−1.42	−2.93	2.51
P2/S2	557	2.23	1.17	−5.52	−1.37	−2.98	2.54
P2/S3	581	2.13	1.03	−5.38	−1.31	−3.04	2.34
P2/S4	589	2.11	1.08	−5.43	−1.35	−3.00	2.42

[a] Absorption wavelengths obtained in solid films and optical band-gaps calculated from the equation of $E_{g,opt} = 1240/\lambda_{edge}$.
[b] Onset oxidation and reduction potentials.
[c] $E_{HOMO}/E_{LUMO} = [-(E_{onset}-0.45)-4.8]$ eV where 0.45 V is the value of ferrocene versus Ag/Ag^+ and 4.8 eV is the energy level of ferrocene below the vacuum.

PSC devices are shown in Figure 9. Under the white-light illumination, the short circuit current density (I_{sc}), open circuit voltage (V_{oc}), fill factor (FF), and PCE values of the PSC devices composed of H-bonded polymer complexes were in the range of 0.42–3.17 mA/cm^2, 0.38–0.59 V, and 24–34%, 0.06–0.50%, respectively.

The photovoltaic properties of the PSC devices containing H-bonded polymer complexes **P1/S1–P1/S4** and **P2/S1–P2/S4** were dependent on the solubility and film-forming quality of the H-bonded complexes. However, the PCE values of H-bonded complexes **P2/S1–P2/S4** containing H-acceptor copolymer **P2** were apparently smaller than those of **P1/S1–P1/S4**, respectively, because the 1:1 M ratio of pyridyl and acid units of fully H-bonded **P2/S1–P2/S4** would reduce the content of low-band-gap dyes complexed with H-acceptor copolymer **P2** bearing 50 mol % of pyridyl units. As shown in Table 4, both series of H-bonded complexes (**P1/S1–P1/S4** and **P2/S1–P2/S4**) containing electron donors of end-capping triphenylamine dyes (**S1** and **S3**) had better PCE values than those containing end-capping carbazole dyes

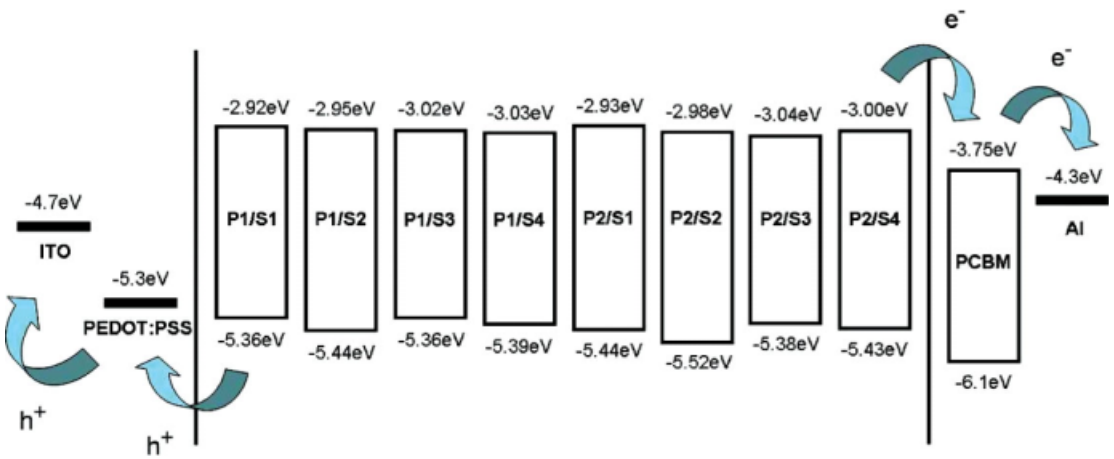

Figure 8. Energy band diagram with HOMO/LUMO levels of H-bonded polymer complexes **P1/S1–P1/S4** (as electron donors) and PCBM (as an electron acceptor) in relation to the work functions of ITO, PEDOT:PSS, and Al (HOMO value of PCBM was obtained from ref. 23). [Color figure can be viewed in the online issue, which is available at www.interscience.wiley.com.]

Table 4. Photovoltaic Properties of PSC Devices Containing an Active Layer of H-Bonded Polymer Complexes:PCBM = 1:1 (w/w) with a Device Configuration of ITO/PEDOT:PSS/H-Bonded Polymer Complexes:PCBM/Ca/Al[a]

Active Layer[b] H-Bonded Complexes: PCBM	V_{oc} (V)	I_{sc} (mA/cm^2)	FF (%)	PCE (%)
P1/S1[c]	0.59	1.67	27	0.28
P1/S2	0.54	1.72	28	0.26
P1/S3	0.47	3.17	34	0.50
P1/S4	0.43	1.70	26	0.19
P2/S1	0.58	0.95	24	0.13
P2/S2	0.53	0.42	27	0.06
P2/S3	0.51	2.29	28	0.32
P2/S4	0.38	0.73	24	0.07

[a] Measured under AM 1.5 irradiation, 100 mW/cm^2.
[b] H-Bonded Polymer Complexes:PCBM = with the fixed weight ratio of 1:1 (w/w).
[c] PCE of **P1/S1P**: 0.16%.

(**S2** and **S4**), respectively. It might be due to the larger aggregations of end-capping carbazole dyes (**S2** and **S4**) to reduce the PCE values, which were confirmed by the redder shifted maximum absorption wavelengths ($\Delta\lambda_{abs} = \lambda_{abs,solid} - \lambda_{abs,solution}$) in solid films of end-capping carbazole dyes ($\Delta\lambda_{abs}$ = 16 nm for **S2** and $\Delta\lambda_{abs}$ = 30 nm for **S4**) than those of end-capping triphenylamine dyes ($\Delta\lambda_{abs}$ = 11 nm for **S1** and $\Delta\lambda_{abs}$ = 23 nm for **S3**), respectively. Among the PSC devices containing H-bonded polymer complexes, those composed of H-donor dye **S3**, i.e., **P1/S3** and **P2/S3**, had the best photovoltaic performance with enhanced I_{sc} values in the corresponding H-bonded complexes **P1/S1–P1/S4** and **P2/S1–P2/S4**, respectively, which might be due to the promoted solubility and better film-forming capability of **S3**. Ideally, the I_{sc} values were determined by the product of the photoinduced charge carrier densities and the charge carrier mobilities within the organic semiconductors.[11] Thus, it can be recognized that the better results of I_{sc} and FF in the PSC device containing **P1/S3** and **P2/S3** were obtained likely due to the well-balanced charge flow and less significant recombination loss[24,55] originated from the highly order structural packing of alkyl side chains. However, the relatively low I_{sc} and FF values in the PSC devices containing **P1/S4** and **P2/S4** were poorly understood at this time, but it might be related to the largest aggregation of **S4** (with the reddest shifted maximum absorption wavelengths in solid, $\Delta\lambda_{abs}$ = 30 nm) and geminate charge recombination at the interface due to stable charge-transfer states, which limited the values of the photocurrents.[56] Though V_{oc} values were related to the differences between the HOMO energy levels of the polymers and the LUMO energy levels of the acceptors,[57] but it was not noticeably varied among the PSC devices containing H-bonded complexes. In addition, the *I–V* curves and photovoltaic properties of dyes **S1–S4** without complexation with the polymers are illustrated in Figure S4 and Table S3 (refer the Supporting Information), which can be compared with the PCE values

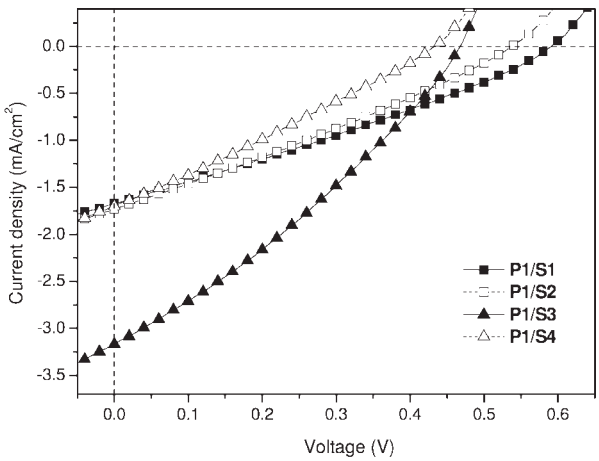

(a)

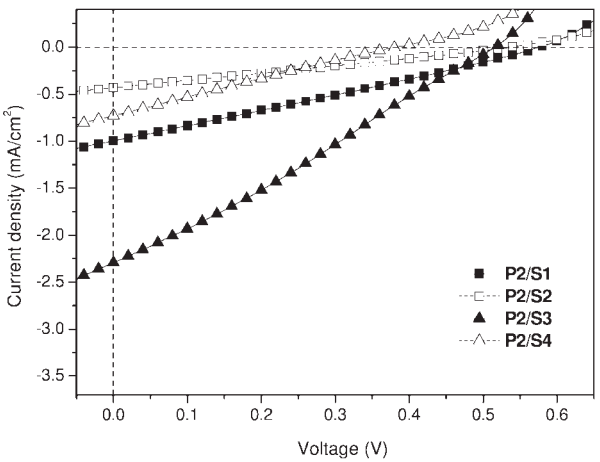

(b)

Figure 9. *I–V* curves (under simulated AM 1.5 solar irradiation) dependencies of PSC devices with an active layer of blended (a) H-bonded polymer complexes **P1/S1–P1/S4**:PCBM (1:1 w/w) and (b) H-bonded polymer complexes **P2/S1–P2/S4**:PCBM (1:1 w/w).

shown in Table 4. In general, the H-bonded polymer complexes containing H-acceptor polymers (**P1** and **P2**) have higher PCE values for the organic solar cells, even though the corresponding dye contents of **S1–S4:**PCBM = 1:1 (w/w) without complexation with polymers in the active layer were almost doubled than those of H-bonded polymer complexes (H-bonded polymer complexes:PCBM = 1:1 w/w). Hence, H-acceptor polymers (**P1** and **P2**) do really improve and facilitate the fabrication of solar cells. To demonstrate the contribution of supramolecular structures in H-bonded polymer complexes, one more PSC device containing an active layer of physical blend **P1/S1P** (without H-bonds) has been fabricated to compare their photovoltaic properties with those of H-bonded polymer complex **P1/S1**. Compared with H-bonded polymer complex **P1/S1** (PCE = 0.28%), physical blend **P1/S1P** (without H-bonds) has a smaller PCE value (0.16%) in Figure S4 and Table S5 (refer the Supporting Information). The larger aggregations of the acid-protected dye **S1P** occurred in the polymer blend **P1/S1P** due to the lack of H-bonding interactions, which also can be confirmed by the red-shifted (33 nm) absorption of polymer blend **P1/S1P** in contrast to that of H-bonded polymer complex **P1/S1** in solid films.

Since the best performance of PSC device (with the highest PCE value in Table 4) was fabricated by the blend of H-bonded polymer complex **P1/S3**:PCBM (1:1 w/w), the current–voltage characteristics of PSC devices as a function of the weight ratio in H-bonded complex and PCBM were surveyed, and their photovoltaic properties are

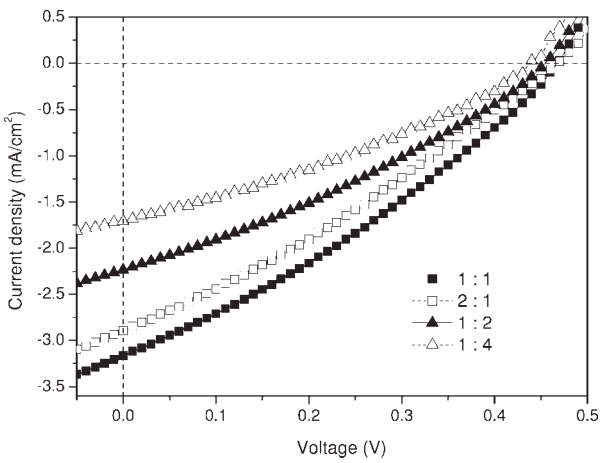

Figure 10. *I–V* curves of PSC devices containing an active layer of H-bonded polymer complex **P1/S3**:PCBM (w/w) with different weight ratios under simulated AM 1.5 solar irradiation.

Table 5. Photovoltaic Parameters for Bulk-Heterojunction PSC Devices Containing Different Weight Ratios of Blended H-Bonded Polymer Complex **P1/S3**:PCBM[a]

Weight Ratios of Blended H-Bonded Complex **P1/S3**:PCBM	V_{oc} (V)	I_{sc} (mA/cm^2)	FF (%)	PCE (%)
2:1	0.46	2.90	20	0.40
1:1	0.47	3.17	34	0.50
1:2	0.45	2.23	30	0.28
1:4	0.44	1.70	33	0.25

[a] PSC devices with the configuration of ITO/PEDOT:PSS/H-Bonded Polymer Complex **P1/S3**:PCBM/Ca/Al containing an active blended layer composed of various weight ratios of H-bonded polymer complex **P1/S3** and PCBM were measured under AM 1.5 irradiation, 100 mW/cm^2.

shown in Figure 10 and Table 5. The optimum photovoltaic performance with the maximum PCE value of 0.50% (I_{sc} = 3.17 mA/cm^2, V_{oc} = 0.47 V, FF = 34%) was obtained in the PSC device having a weight ratio of **P1/S3**:PCBM = 1:1. Using lower weight ratios of PCBM in blended H-bonded polymer complex **P1/S3**:PCBM (2:1 w/w) led to the reduction in I_{sc} values due to the inefficient charge separation and electron transporting properties by the possibly increased aggregation of H-bonded complex **P1/S3**, resulting in the lower PCE results.[58] However, loading larger weight ratios of PCBM in blended H-bonded polymer complex **P1/S3**:PCBM (1:2 and 1:4 w/w) also reduced the I_{sc} and PCE values, which could be probably attributed to the increased aggregation of PCBM so as to affect the separation of charges. Moreover, an unbalanced charge transporting property would be introduced due to the large PCBM ratio. Hence, both I_{sc} and PCE values decreased with larger PCBM molar ratios of 1:2 and 1:4 (w/w) because of the two reasons described here.[59] Overall, the PSC device fabricated by H-bonded polymer complexes **P1/S3**:PCBM (1:1 w/w) reached the highest PCE of 0.50%, with a short circuit current density (I_{sc}) of 3.17 mA/cm^2, an open circuit voltage (V_{oc}) of 0.47 V, and a fill factor (FF) of 0.34.

CONCLUSIONS

In conclusion, novel supramolecular side-chain polymers (i.e., H-bonded polymer complexes) were

constructed by complexation of pyridyl H-acceptor polymers with low-band-gap H-donor dyes in a molar ratio of 1:1 for pyridyl and acid units, which would have much more uptaken loads of photovoltaic dyes in the supramolecular polymeric structures compared with the normal polymer blends. Because of the lack of supramolecular interactions, the larger aggregations of the acid-protected dyes occurred in the polymer blends, and thus a polymer blend (without H-bonds) containing conjugated H-acceptor polymer **P1** and acid-protected dye **S1P** illustrated an obvious reduction in the PCE value in contrast to the supramolecular analogue **P1/S1**. H-donor dyes (**S1–S4**) and H-acceptor polymers (**P1** and **P2**) were utilized to control the mesomorphic, photophysical, and photovoltaic properties effectively by the concept of supramolecular architecture. The supramolecular architectures of H-bonded side-chain polymers were also confirmed by FTIR and XRD measurements. The nematic phase was observed by the introduction of various H-donor dyes and H-acceptor polymers with corresponding supramolecular side-chain structures. In addition, compared with H-donor dyes, the optical properties demonstrated that blue-shifted absorptions occurred in these H-bonded complexes as the H-donor dyes were complexed with H-acceptor polymers. Thus, the electrochemical properties of H-bonded complexes were adjusted by introducing electron-withdrawing cyano groups and electron-donating amine groups of H-donor dyes to the H-bonded complexes, which could reduce the HOMO energy levels and increase the LUMO energy levels of the H-bonded side-chain polymers, and thus, to have narrower band-gaps than H-acceptor polymers. Because of the reduced content of low-band-gap dyes complexed with H-acceptor copolymer **P2**, the PCE values of H-bonded complexes **P2/S1–P2/S4** containing H-acceptor copolymer **P2** were apparently smaller than those of **P1/S1–P1/S4**, respectively. Preliminary PSC devices based on these H-bonded polymer complex **P1/S3** blended with PCBM acceptors (1:1 w/w) had the PCE up to 0.50%, which gave the best performance with the values of $I_{sc} = 3.17$ mA/cm^2, $V_{oc} = 0.47$ V, and FF = 34%.

The authors are grateful to the National Center for High-performance Computing for computer time and facilities. The powder XRD measurements are supported by beamline BL17A (charged by J.-J. Lee) of the National Synchrotron Radiation Research Center (NSRRC), in Taiwan. The financial supports of this project provided by the National Science Council of Taiwan (ROC) through NSC 97-2113*M*-009-006-MY2, National Chiao Tung University through 97W807, and Energy and Environmental Laboratories (charged by C.-C. Yang) in Industrial Technology Research Institute (ITRI) are acknowledged.

REFERENCES AND NOTES

1. Ikkala, O.; Brinke, G. T. Science 2002, 295, 2407–2409.
2. Stupp, S. I.; Son, S.; Lin, H. C.; Li, L. S. Science 1993, 259, 59–63.
3. Kato, T.; Mizoshita, N.; Kishimoto, K. Angew Chem Int Ed 2006, 45, 38–68.
4. (a) Broeren, M. A. C.; Linhardt, J. G.; Malda, H.; de Waal, B. F. M.; Versteegen, R. M.; Meijer, J. T.; Löwik, D. W. P. M.; van Hest, J. C. M.; van Genderen, M. H. P.; Meijer, E. W. J Polym Sci Part A: Polym Chem 2005, 43, 6431–6437; (b) Montarnal, D.; Cordier, P.; Soulié-Ziakovic, C.; Tournilhac, F.; Leibler, L. J Polym Sci Part A: Polym Chem 2008, 46, 7925–7936; (c) Vellis, P. D.; Mikroyannidis, J. A.; Lo, C. N.; Hsu, C. S. J Polym Sci Part A: Polym Chem 2008, 46, 7702–7712; (d) Cheng, C. C.; Huang, C. F.; Yen, Y. C.; Chang, F. C. J Polym Sci Part A: Polym Chem 2008, 46, 6416–6424; (e) Coluccini, C.; Metrangolo, P.; Parachini, M.; Pasini, D.; Resnati, G.; Righetti, P. J Polym Sci Part A: Polym Chem 2008, 46, 5202–5213; (f) Bosman, A. W.; Sijbesma, R. P. J Polym Sci Part A: Polym Chem 2008, 46, 3877–3885; (g) Aamer, K. A.; Tew, G. N. J Polym Sci Part A: Polym Chem 2007, 45, 1109–1121; (h) Stefopoulos, A. A.; Pefkianakis, E. K.; Papagelis, K.; Andreopoulou, A. K.; Kallitsis, J. K. J Polym Sci Part A: Polym Chem 2009, 47, 2551–2559.
5. Pisula, W.; Tomović, Ž.; Wegner, M.; Graf, R.; Pouderoijen, M. J.; Meijer, E. W.; Schenning, A. P. H. J. J Mater Chem 2008, 18, 2968–2977.
6. (a) Vera, F.; Almuzara, C.; Orera, I.; Barberá, J.; Oriol, L.; Serrano, J. L.; Sierra, T. J Polym Sci Part A: Polym Chem 2008, 46, 5528–5541; (b) Fustin, C. A.; Guillet, P.; Misner, M. J.; Russell, T. P.; Schubert, U. S.; Gohy, J. F. J Polym Sci Part A: Polym Chem 2008, 46, 4719–4724; (c) Guillet, P.; Fustin, C. A.; Lohmeijer, B. G. G.; Schubert, U. S.; Gohy, J. F. Macromolecules 2006, 39, 5484–5488; (d) Fustin, C. A.; Guillet, P.; Schubert, U. S.; Gohy, J. F. Adv Mater 2007, 19, 1665–1673; (d) Burke, K. A.; Sivakova, S.; McKenzie, B. M.; Mather, P. T.; Rowan, S. J. J Polym Sci Part A: Polym Chem 2006, 44, 5049–5059.
7. Kato, T.; Matsuoka, T.; Nishii, M.; Kamikawa, Y.; Kanie, K.; Nishimura, T.; Yashima, E.; Ujiie, S. Angew Chem Int Ed 2004, 43, 1969–1972.

8. Mamlouk, H.; Heinrich, B.; Bourgogne, C.; Donnio, B.; Guillon, D.; Felder-Flesch, D. J Mater Chem 2007, 17, 2199–2205.
9. (a) Wanunu, M.; Popovitz-Biro, R.; Cohen, H.; Vaskevich, A.; Rubinstein, I. J Am Chem Soc 2005, 127, 9207–9215; (b) Obare, S. O.; Hollowell, R. E.; Murphy, C. J. Langmuir 2002, 18, 10407–10410.
10. Winder, N. S.; Saridifti, N. S. J Mater Chem 2004, 14, 1077–1086.
11. Günes, S.; Neugebauer, H.; Sariciftci, N. S. Chem Rev 2007, 107, 1324–1338.
12. Yang, X.; Loos, J. Macromolecules 2007, 40, 1353–1362.
13. Granstrom, M.; Petritsch, K.; Arias, A. C.; Lux, A.; Andersson, M. R.; Friend, R. H. Nature 1998, 395, 257–260.
14. Halls, J. J. M.; Walsh, C. A.; Greenham, N. C.; Marseglia, E. A.; Friend, R. H.; Moratti, S. C.; Holmes, A. B. Nature 1995, 376, 498–500.
15. Kietzke, T.; Hörhold, H.-H.; Neher, D. Chem Mater 2005, 17, 6532–6537.
16. Breeze, A. J.; Salomon, A.; Ginley, D. S.; Gregg, B. A.; Tillmann, H.; Hörhold, H.-H. Appl Phys Lett 2002, 81, 3085–3087.
17. Yu, G.; Gao, J.; Hummelen, J. C. Science 1995, 270, 1789–1791.
18. Brabec, C. J.; Sariciftci, N. S.; Hummelen, J. C. Adv Funct Mater 2001, 11, 15–26.
19. Al-Ibrahima, M.; Rotha, H. K.; Zhokhavetsb, U. Sol Energy Mater Sol Cells 2005, 85, 13–20.
20. Ma, W.; Yang, C.; Gong, X.; Lee, K.; Heeger, A. J. Adv Funct Mater 2005, 15, 1617–1622.
21. Lindner, S. M.; Hüttner, S.; Chiche, A.; Thelakkat, M.; Krausch, G. Angew Chem Int Ed 2006, 45, 3364–3368.
22. Peet, J.; Kim, J. Y.; Coates, N. E.; Ma, W. L.; Moses, D.; Heeger, A. J.; Bazan, G. C. Nat Mater 2007, 6, 497–500.
23. Mülhlbacher, D.; Scharber, M.; Morana, M.; Zhu, Z.; Waller, D.; Gaudiana, R.; Brabec, C. Adv Mater 2006, 18, 2884–2889.
24. Zhu, Z.; Waller, D.; Gaudiana, R.; Morana, M.; Mülhlbacher, D.; Scharber, M.; Brabec, C. Macromolecules 2007, 40, 1981–1986.
25. Huo, L.; He, C.; Han, M.; Zhou, E.; Li, Y. F. J Polym Sci Part A: Polym Chem 2007, 45, 3861–3871.
26. Colladet, K.; Fourier, S.; Cleij, T. J.; Lutsen, L.; Gelan, J.; Vanderzande, D. Macromolecules 2007, 40, 65–72.
27. Shahid, M.; Ashraf, R. S.; Klemm, E.; Sensfuss, S. Macromolecules 2006, 39, 7844–7853.
28. Zhan, X.; Tan, Z.; Domercq, B.; An, Z.; Zhang, X.; Barlow, S.; Li, Y.; Zhu, D.; Kippelen, B.; Marder, S. R. J Am Chem Soc 2007, 129, 7246–7247.
29. Zhu, Y.; Champion, R. D.; Jenekhe, S. A. Macromolecules 2006, 39, 8712–8719.
30. Champion, R. D.; Cheng, K. F.; Pai, C. L.; Chen, W. C.; Jenekhe, S. A. Macromol Rapid Commun 2005, 26, 1835–1840.
31. Gebeyehu, D.; Pfeiffer, M.; Maennig, B.; Drechsel, J.; Werner, A.; Leo, K. Thin Solid Films 2004, 451–452, 29–32.
32. (a) Shin, R. Y. C.; Kietzke, T.; Sudhakar, S.; Chen, Z. K.; Dodabalapur, A.; Sellinger, A. Chem Mater 2007, 19, 1892–1894; (b) Kietzke, T.; Shin, R. Y. C.; Egbe, D. A. M.; Chen, Z. K.; Sellinger, A. Macromolecules 2007, 40, 4424–4428; (c) Ooi, Z. E.; Tam, T. L.; Shin, R. Y. C.; Chen, Z. K.; Kietzke, T.; Sellinger, A.; Baumgarten, M.; Mullene, K.; deMello, J. C. J Mater Chem 2008, 18, 4619–4622; (d) Mei, J.; Heston, N. C.; Vasilyeva, S. V.; Reynolds, J. R. Macromolecules 2009, 42, 1482–1487.
33. (a) Fan, B.; Hany, R.; Moser, J. E.; Nüesch, F. Org Electron 2008, 9, 85–94; (b) Belcher, W. J.; Wagner, K. I.; Dastoor, P. C. Sol Energy Mater Sol Cells 2007, 91, 447–452; (c) Suresh, P.; Balaraju, P.; Sharma, S. K.; Roy, M. S.; Sharma, G. D. Sol Energy Mater Sol Cells 2008, 92, 900–908; (d) Wang, M.; Wang, X. Sol Energy Mater Sol Cells 2007, 91, 1782–1787.
34. (a) Wang, M.; Wang, X. Sol Energy Mater Sol Cells 2008, 92, 766–771; (b) Castro, F. A.; Faes, A.; Geiger, T.; Graeff, C. F. O.; Nagel, M.; Nüesch, F.; Hany, R. Synth Metal 2005, 155, 51–55; (c) Guo, X.; Bu, L.; Zhao, Y.; Xie, Z.; Geng, Y.; Wang, L. Thin Solid Films 2009, 517, 4654–4657; (d) Bouclé, J.; Chyla, S.; Shaffer, M. S. P.; Durrant, J. R.; Bradley, D. D. C.; Nelson, J. Adv Funct Mater 2008, 18, 622–633.
35. (a) van Mullekom, H. A. M.; Vekemans, J. A. J. M.; Havinga, E. E.; Meijer, E. W. Mater Sci Eng 2001, 32, 1–40; (b) Lim, Y. F.; Shu, Y.; Parkin, S. R.; Anthony, J. E.; Malliaras, G. G. J Mater Chem 2009, 19, 3049–3056; (c) Roquet, S.; Cravino, A.; Leriche, P.; Alévêque, O.; Frère, P.; Roncali, J. J Am Chem Soc 2006, 128, 3459–3466; (d) Yasuda, T.; Imase, T.; Nakamura, Y.; Yamamoto, T. Macromolecules 2005, 38, 4687–4697; (e) Zhang, Z. G.; Zhang, K. L.; Liu, G.; Zhu, C. X.; Neoh, K. G.; Kang, E. T. Macromolecules 2009, 42, 3104–3111; (f) Li, K. C.; Hsu, Y. C.; Lin, J. T.; Yang, C. C.; Wei, K. H.; Lin, H. C. J Polym Sci Part A: Polym Chem 2008, 46, 4285–4304; (g) Li, K. C.; Hsu, Y. C.; Lin, J. T.; Yang, C. C.; Wei, K. H.; Lin, H. C. J Polym Sci Part A: Polym Chem 2009, 47, 2073–2092; (h) Li, K. C.; Huang, J. H.; Hsu, Y. C.; Huang, P. J.; Chu, C. W.; Lin, J. T.; Ho, K. C.; Wei, K. H.; Lin, H. C. Macromolecules 2009, 42, 3681–3693.
36. Shen, Z.; Strauss, J.; Daub, J. Chem Commun 2002, 5, 460–461.
37. Lai, R. Y.; Kong, X.; Jenekhe, S. A.; Bard, A. J. J Am Chem Soc 2003, 125, 12631–12639.

38. Liu, Y.; Cao, H.; Li, J.; Chen, Z.; Cao, S.; Xiao, L.; Xu, S.; Gong, Q. J Polym Sci Part A: Polym Chem 2007, 45, 4867–4878.
39. Yang, L. Y.; Wang, C.; Li, L. Q.; Janietz, S.; Wedel, A.; Hua, Y. L.; Yin, S. G. J Polym Sci Part A: Polym Chem 2007, 45, 4291–4299.
40. Cho, N. S.; Park, J. H.; Lee, S. K.; Lee, J.; Shim, H. K. Macromolecules 2006, 39, 177–183.
41. Tang, W.; Kietzke, T.; Vemulamada, P.; Chen, Z. K. J Polym Sci Part A: Polym Chem 2007, 45, 5266–5276.
42. Zou, Y.; Wu, W.; Sang, G.; Yang, Y.; Liu, Y.; Li, Y. Macromolecules 2007, 40, 7231–7237.
43. Roncali, J. Chem Rev 1997, 97, 173–206.
44. Tu, G.; Li, H.; Forster, M.; Heiderhoff, R.; Balk, L. J.; Scherf, U. Macromolecules 2006, 39, 4327–4331.
45. (a) Velusamy, M.; Thomas, K. R. J.; Lin, J. T.; Hsu, Y. C.; Ho, K. C. Org Lett 2005, 7, 1899–1902; (b) Thomas, K. R. J.; Hsu, Y. C.; Lin, J. T.; Lee, K. M.; Ho, K. C.; Lai, C. H.; Cheng, Y. M.; Chou, P. T. Chem Mater 2008, 20, 1830–1840; (c) Tsai, M. S.; Hsu, Y. C.; Lin, J. T.; Chen, H. C.; Hsu, C. P. J Phys Chem C 2007, 111, 18785–18793; (d) Thomas, K. R. J.; Lin, J. T.; Hsu, Y. C.; Ho, K. C. Chem Commun 2005, 4098–4100; (e) Lin, J. T.; Chen, P. C.; Yen, Y. S.; Hsu, Y. C.; Chou, H. H.; Yeh, M. C. P. Org Lett 2009, 11, 97–100.
46. (a) Koumura, N.; Wang, Z. S.; Mori, S.; Miyashita, M.; Suzuki, E.; Hara, K. J Am Chem Soc 2006, 128, 14256–14257; (b) Wang, Z. S.; Koumura, N.; Cui, Y.; Takahashi, M.; Sekiguchi, H.; Mori, A.; Kubo, T.; Furube, A.; Hara, K. Chem Mater 2008, 20, 3993–4003; (c) Kim, J. J.; Choi, H.; Lee, J. W.; Kang, M. S.; Song, K.; Kang, S. O.; Ko, J. J Mater Chem 2008, 18, 5223–5229; (d) Wang, Z. S.; Cui, Y.; Dan-oh, Y.; Kasada, C.; Shinpo, A.; Hara, K. J Phys Chem C 2007, 111, 7224–7230.
47. Lin, H. C.; Tsai, C. M.; Huang, G. H.; Tao, Y. T. Macromolecules 2006, 39, 557–568.
48. Wu, C. W.; Lin, H. C. Macromolecules 2006, 39, 7985–7997.
49. Lin, H. C.; Jiang, M. D.; Wu, S. C.; Jou, L. L.; Chou, K. P.; Huang, C. M.; Wei, K. H. J Polym Sci Part A: Polym Chem 2009, 47, 4685–4702.
50. Liang, T. C.; Lin, H. C. J Polym Sci Part A: Polym Chem 2009, 47, 2734–2753.
51. Yang, P. J.; Wu, C. W.; Sahu, D.; Lin, H. C. Macromolecules 2008, 41, 9692–9703.
52. Chen, C. P.; Chan, S. H.; Chao, T. C.; Ting, C.; Ko, B. T. J Am Chem Soc 2008, 130, 12828–12833.
53. Lee, J. Y.; Painter, P. C.; Coleman, M. M. Macromolecules 1988, 21, 954–960.
54. Roncali, J. Macromol Rapid Commun 2007, 28, 1761–1775.
55. Huo, L.; Tan, Z.; Wang, X.; Zhou, Y.; Han, M. F.; Li, Y. F. J Polym Sci Part A: Polym Chem 2008, 46, 4038–4049.
56. Morteani, A. C.; Sreearunothai, P.; Herz, L. M.; Friend, R. H.; Silva, C. Phys Rev Lett 2004, 92, 247402–247404.
57. (a) Scharber, M. C.; Mühlbacher, D.; Koppe, M.; Denk, P.; Waldauf, C.; Heeger, A. J.; Brabec, C. J. Adv Mater 2006, 18, 789–794; (b) Brabec, C. J.; Cravino, A.; Meissner, D.; Sariciftci, N. S.; Fromherz, T.; Rispens, M. T.; Sanchez, L.; Hummelen, J. C. Adv Funct Mater 2001, 11, 374–380.
58. Baek, N. S.; Hau, S. K.; Yip, H. L.; Acton, O.; Chen, K. S.; Jen, A. K. Y. Chem Mater 2008, 20, 5734–5736.
59. Huang, J. H.; Ho, Z. Y.; Kekuda, D.; Chang, Y.; Chu, C. W.; Ho, K. C. Nanotechnology 2009, 20, 025202.